ACS OMEGA

Open Access

http://pubs.acs.org/journal/acsodf

Article

Investigating Pyruvate Dehydrogenase Kinase 3 Inhibitory Potential of Myricetin Using Integrated Computational and Spectroscopic Approaches

Saleha Anwar, Shama Khan, Afzal Hussain, Mohamed F. Alajmi, Anas Shamsi,* and Md. Imtaiyaz Hassan*

Cite This: *ACS Omega* 2024, 9, 29633−29643

Read Online

ACCESS | Metrics & More | Article Recommendations

ABSTRACT: Protein kinases are involved in various diseases and currently represent potential targets for drug discovery. These kinases play major roles in regulating the cellular machinery and control growth, homeostasis, and cell signaling. Dysregulation of kinase expression is associated with various disorders such as cancer and neurodegeneration. Pyruvate dehydrogenase kinase 3 (PDK3) is implicated in cancer therapeutics as a potential drug target. In this current study, a molecular docking exhibited a strong binding affinity of myricetin to PDK3. Further, a 100 ns all-atom molecular dynamics (MD) simulation study provided insights into the structural dynamics and stability of the PDK3-myricetin complex, revealing the formation of a stable complex with minimal structural alterations upon ligand binding. Additionally, the actual affinity was ascertained by fluorescence binding studies, and myricetin showed appreciable binding affinity to PDK3. Further, the kinase inhibition assay suggested significant inhibition of PDK3 by myricetin, revealing an excellent inhibitory potential with an IC_{50} value of 3.3 μM. In conclusion, this study establishes myricetin as a potent PDK3 inhibitor that can be implicated in therapeutic targeting cancer and PDK3-associated diseases. In addition, this study underscores the efficacy of myricetin as a potential lead to drug discovery and provides valuable insights into the inhibition mechanism, enabling advancements in cancer therapeutics.

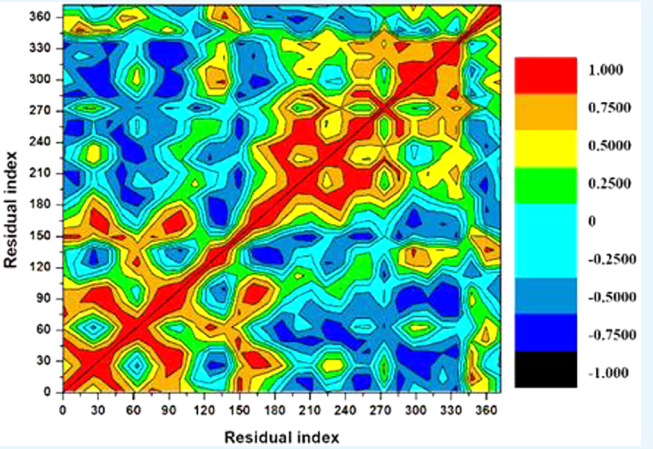

INTRODUCTION

Cancer is defined as the uncontrolled growth of cells characterized by changes in the cellular machinery, including various hallmarks. One hallmark is modulated glucose metabolism in aerobic conditions, termed "aerobic glycolysis".[1] In typical, healthy cells, glucose undergoes glycolysis to produce pyruvate, subsequently metabolized in the mitochondria through oxidative phosphorylation to generate a significant amount of adenosine triphosphate (ATP), serving as the cell's primary source of energy. However, in many cancer cells, glycolysis is intensified and the resulting pyruvate is frequently transformed into lactate, even when oxygen is readily available. This metabolic shift enables cancer cells to satisfy their energy requirements and facilitate their rapid growth and proliferation, termed the Warburg effect.[2]

Aerobic glycolysis is a favorable metabolic switch in cancer, redirecting energy production toward glycolysis and supporting its survival through various mechanisms. In contrast, oxidative phosphorylation (OXPHOS) is the predominant energy source in normal cells. The inhibition of the pyruvate dehydrogenase complex (PDHC) and the reliance on glycolysis as the main energy source result in the buildup of cytoplasmic lactate, a condition referred to as "cell acidosis". The acidic cellular environment additionally provides cancer cells with advantages for their survival.[3,4] Despite notable progress in cancer therapeutics, the disease is ranked as the second leading cause of death. The inadequacy of current treatment methods can be associated to various factors, including the development of multidrug resistance.[5]

Protein kinases (PKs) make up a subgroup of proteins that collectively function to phosphorylate other targets. These PKs utilize ATP as a source of phosphate by breaking down ATP

Received: March 28, 2024
Revised: May 13, 2024
Accepted: June 7, 2024
Published: June 26, 2024

into ADP and harnessing the liberated γ-phosphate.[6] The human genome contains over 500 protein kinases, with 478 classified as classical PKs and 40 classified as atypical PKs. The phosphorylation process carried out by these PKs plays a pivotal role in governing diverse cellular functions. Changes in kinase activity can result in various modifications to the normal functioning of the cellular processes. Furthermore, the aberrant activity of protein kinases is a recognized characteristic linked to cancer initiation, progression, and spread.[7] PKs are integral components of numerous signaling pathways, exhibit elevated expression levels, and play a role in activating multiple oncogenic pathways. The creation and advancement of potent kinase inhibitors have become a promising field in cancer therapeutics.[8] A substantial portion of cellular pathways is under the control of PKs, as the process of phosphorylation and dephosphorylation fine-tunes the operation of these pathways. Aberrations in their functionality are typically linked to the initiation of various diseases.[9] Over the last few decades, PKs have garnered interest as potential targets in treating cancer, metabolic syndromes, neurodegenerative conditions, and various diseases.[10−12] The FDA-approved inhibitors have been developed for some of these kinases. Additionally, a range of small-molecule inhibitors targeting protein kinases are currently at various stages of clinical trials.[13]

The pyruvate dehydrogenase complex (PDHC) is a notable complex involved in glucose regulation and energy generation in mammals. This complex acts as a link connecting glycolysis with the TCA cycle.[14] The efficient functioning of the complex relies on coordination between PDKs and phosphatases. PDKs facilitate phosphorylation of specific serine residues on the E1α subunit of PDHC, further deactivating the complex.[15,16] The association of PDK3 leads to its inactivation of PDHC, which is linked to the development of several cancer types.[17] The PDK3 protein exhibits increased expression under the influence of various factors, primarily due to the unregulated transcription induced by hypoxia-inducible factor-1α (HIF-1α). The heightened levels of this kinase lead to the inhibition of mitochondrial respiration processes, causing alterations in energy production responsibilities.[18] Pyruvate is involved in a negative feedback mechanism with PDKs 1, 2, and 4. Interestingly, there is no feedback loop between pyruvate and PDK3.[16] This distinctive characteristic of PDK3 amplifies its role in supporting cancer survival.[19] The observed correlation between increased PDK3 expression and improved cancer survival underscores the significance of inhibiting the expression of PDK3. Ongoing research is focused on developing drugs to inhibit this kinase through drug discovery.[20,21] The binding site of PDK3 is a region on the surface of the protein, where it interacts with its substrates and inhibitors. In PDK3, certain aspartate (Asp) residues participate in deprotonation of the substrate or in stabilization of transition states during phosphorylation. Serine (Ser) and threonine (Thr) residues are often phosphorylated during enzyme activity. In PDK3, specific Ser or Thr residues may serve as phosphorylation sites that are targeted by upstream kinases or participate directly in the phosphorylation of the PDC.

In recent years, there has been growing interest in exploring natural products as a source of potential treatments. Phytochemicals derived from plants have demonstrated their efficacy as potent agents in various diseases, offering therapeutic benefits with minimal side effects.[22−26] Phytochemicals exhibit significant diversity and have been employed for various health purposes throughout history.[27] Phytochemicals encompass varied chemical compounds with powerful anticancer potential. Several of these compounds have received approval for their use against cancer.[28,29]

Myricetin (MT) is a potent natural compound associated with managing diseases due to its antimicrobial, anti-inflammatory, cardioprotective, and antidiabetic properties.[30,31] Its impact on different types of cancer has been elucidated through its ability to modulate crucial cell-signaling molecules. Recent studies highlight MT's potential in cancer management by targeting various cancer hallmarks through diverse molecular mechanisms. This flavonoid has been shown to inhibit cell proliferation, angiogenesis, and metastasis while inducing apoptosis.[32,33] Numerous investigations have revealed that PDK3 is upregulated in a variety of cancer types, and a correlation has been observed between elevated PDK3 expression and the progression of cancer. In lieu of the powerful anticancer potential of phytochemicals, the study aims to investigate the binding mechanism of MT with PDK3 and further investigate its kinase inhibitory potential. This study is the first of a kind that reports PDK3 as a target of MT, opening up new avenues of using MT in anticancer therapeutics by targeting PDK3.

Initially, we conducted molecular docking studies to assess the interactions between MT and PDK3. Subsequently, we performed molecular dynamics (MD) simulation study over 100 ns, during which we computed all significant parameters related to protein−ligand interactions. We also analyzed variations in the secondary structure over time after ligand binding and conducted MM/GBSA analysis to evaluate the binding's favorability. After this *in-silico* analysis, we examined the impact of the ligand on the protein's structure and activity through ATPase inhibition and fluorescence binding assays. Our results confirm that MT interacts with PDK3 with distinct binding efficiencies. As a result, it may warrant investigation for therapeutic applications following a specific validation process.

MATERIAL AND METHODS

Materials. LB (Luria−Bertani) and LB agar were used in bacterial culturing, purchased from HiMedia. Antibiotics were purchased from Sigma-Aldrich (USA). Chemicals such as CAPS buffer, NaCl, Tris-HCl, NaOH, *N*-lauryl sarcosine, imidazole, etc., were purchased from Merck, Germany. Ni-NTA beads were purchased from Qiagen, Germany. MT was purchased from Sigma-Aldrich, United States. Milli-Q water was used in buffer preparation.

Protein Expression and Purification. The human *PDK3* gene was obtained from the PlasmID HMS library of human kinases. The protein was purified as per our previously established protocols.[34]

Enzyme Inhibition Assay. The malachite-based enzyme assay was done to evaluate the kinase activity of PDK3 by measuring the amount of ATP transformed into ADP and the subsequent release of P*i*. The protein (PDK3) was taken in 5 μM concentration for the assay. The kinase activity without any ligand was considered 100% activity. Further, an increasing concentration of MT was added in different wells of a 96-well plate and incubated for an hour. After the incubation time, ATP was added (200 mM) to all the wells and incubated for 30 min. The reaction was terminated by adding the BIOMOL green reagent and allowed to carry out its function for 20−30 min. The 96-well plate was analyzed spectrophotometrically at

https://doi.org/10.1021/acsomega.4c03001
ACS Omega 2024, 9, 29633−29643

620 nm with a multiplate reader to analyze the changes in activity of the protein kinase.[35]

Fluorescence Binding Assay. Fluorescence measurements are useful for examining the association between biomolecules with small compounds. The aromatic amino acids, especially Tryptophan (Trp) is the main source of intrinsic fluorescence in proteins due to the presenece of Trp residues which is responsible for the fluorescence intensity. Using MT as a ligand, a fluorescence-based binding experiment was performed on PDK3 using a Jasco spectrofluorometer (FP-6200). A stock solution of MT (1 mM) was prepared initially and was diluted further to the working concentrations. The concentration of PDK3 was kept constant at 4 μM, and MT was varied from 0 to 8 μM. The resultant spectra were measured between 300 and 400 nm after PDK3 was stimulated at 280 nm with response set to medium and slit width set at 10 nm. The inner filter effect was accounted for in all experiments, following established protocols.[36] All the spectra reported here are the subtracted spectra after considering the fluorescence of MT by taking the blank spectra of the ligand. A thorough examination of quenching was carried out utilizing the modified Stern−Volmer equation.[37] We carried out these in triplicate, and the mean was taken into account for the calculation.

$$\log \frac{F_0 - F}{F} = \log K + n \log[C] \quad (1)$$

Molecular Docking Studies. Under the PDB identifier code 1Y8O, the atomic coordinates of the human PDK3 protein were retrieved directly from the Protein Data Bank (PDB) database.[38] The Schrödinger package was utilized to compute the PDK3 structure for the docking studies. Getting a neutral pH of 7.0 required removing crystallographic water molecules, adjusting the protein's charge, and adding hydrogen atoms.[39,40] The 2-D structure of MT with CID number 5281672 was obtained from the PubChem database. Schrödinger's LigPrep module optimized the small molecule structure by adding hydrogen atoms and converting it into a 3-D format file to improve its orientation. Subsequently, a receptor grid was generated with coordinates of X = −47.86, Y = 18.59, Z = 69.03, with dimensions of 20 × 20 × 20 Å. Using Schrödinger's Glide module in the extreme precision (XP) mode, molecular docking was performed. After achieving favorable orientations, we further process this MT-PDK3 docked complex for 100 ns of MD simulation to investigate any structural changes in the MT-PDK3 complex to support our preliminary hypothesis.[41]

Molecular Dynamics Simulations. The apo-PDK3 and MT-PDK3 systems were processed through the Graphics Processing Unit (GPU) version of the PMEMD package, supported in Amber-18. Protein termini were capped on both sides with neutral acetyl and methylamide residues to ensure stability during and after the simulations. The Antechamber module was used to parametrize and assign atomic charges to the molecule. Force field ff14SB was implemented on the apo-PDK3 and the MT-PDK3 complex to define the protein. The LEaP module in Amber-18 was used to solvate ions inside the systems.[42−45] A TIP3P water box was chosen as solvent in our intricate model by maintaining a 10 Å distance between the atoms and solutes. A periodic van der Waals cutoff of 12 Å was implemented for efficient and accurate simulations with a 2 fs integration time step. Systems were minimized with a restraint potential of 10 Å using 500 steps steepest descent continuing until 1000 conjugate gradient processes. Afterward, the systems were gradually heated from 0 to 300 K, having a harmonic restraint of 10 Å followed by an equilibration step for 5 ns by removing all the previous restraints. A final production phase run of 100 ns was performed for both apo-PDK3 and the MT-PDK3 complex to analyze the changes in the trajectories. Our most recent articles include more detailed information on the process.[46]

Post-MD Simulation Dynamic Trajectories Investigation. AMBER's CPPTRAJ module was used to perform post-MD analysis on the MT-PDK3 complex and apo-PDK3. This module is important in assessing and working with trajectory data from MD simulation experiments.[47] We assessed the structural alterations in the protein using several analytical techniques such as radius of gyration, solvent accessible surface area, hydrogen bond analysis, root-mean-square deviation, root-mean-square fluctuations, and secondary structure analysis. The Origin plotting tool was utilized to create 2-D graphs from the MD trajectories to display appropriate results.[48]

Dynamic Cross-Correlation Matrix. Using dynamic cross-correlation matrices (DCCM), the MD resultant trajectories were analyzed for residual movement. The changes in the protein's Cα atom can be ascertained using this analysis.[49] Using all the PDK3 backbone Cα atoms, the least-squares-fitting approach is used in DCCM to translate and rotate all configurations to align on the equilibrated configurations after the bound ligand. The methodology used was as per our previous publications.[50] The cross-correlation coefficient C_{ij} was calculated using the below-specified equation, where i and j denote the atomic fluctuations in the systems:

$$C_{ij} = \frac{\langle \Delta r_i \cdot \Delta r_j \rangle}{(\langle \Delta r_i^2 \rangle \langle \Delta r_j^2 \rangle)^{1/2}} \quad (2)$$

The symbol $\Delta r_{i,j}$ represents the deviation of the standard point between the i^{th} and j^{th} molecules, with angle braces denoting the complete bends. All corresponding charges are denoted by $C_{ij} = 1$, while $C_{ij} = -1$ indicates highly resistant developments throughout. The range of changes from 1 to −1 illustrates the correlation and anticorrelation between the activities of i and j. The DCCM was computed using the CPPTRAJ module in Amber 18, and all matrices were visualized using Origin software.

Thermodynamic Free Energy Calculations. Utilizing the molecular mechanics/generalized-Born surface area (MM/GBSA) technique,[51] we computed the MT-PDK3 complex's relative binding free energies. The CPPTRAJ module eliminated all counterions and solvents from the system.[52] The free energies (ΔG_{bind}) were computed using the equation for both systems:

$$\Delta G_{bind} = G_{complex} - G_{protein} - G_{ligand} \quad (3)$$

The free energy term ΔG_{bind} is computed using the following equations:

$$\Delta G_{bind} = \Delta E_{gas} + \Delta G_{solvation} - T\Delta S \quad (4)$$

where

$$\Delta E_{gas} = \Delta E_{int} + \Delta E_{vdw} + \Delta E_{elec} \quad (5)$$

$$\Delta E_{int} = \Delta E_{bond} + \Delta E_{angle} + \Delta E_{torsion} \quad (6)$$

https://doi.org/10.1021/acsomega.4c03001
ACS Omega 2024, 9, 29633−29643

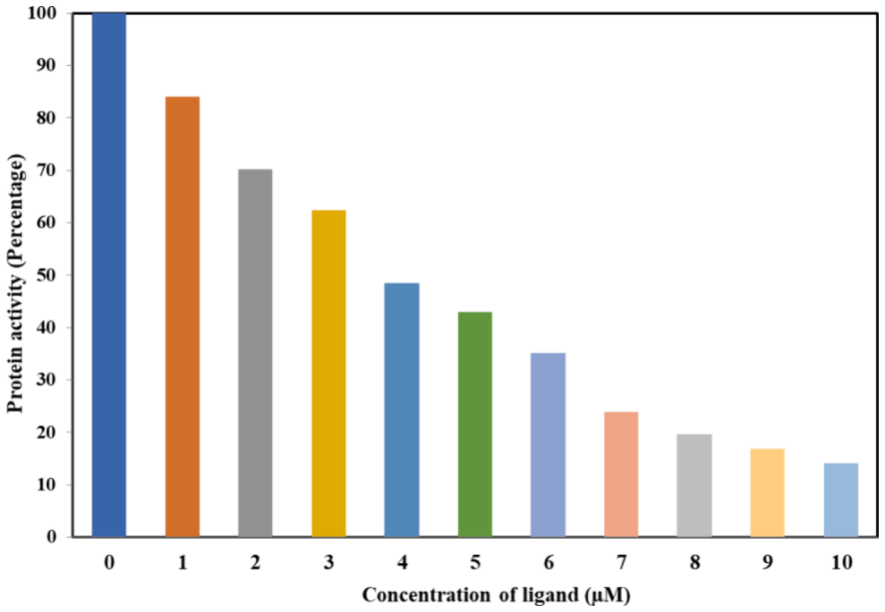

Figure 1. ATPase assay of PDK3 with increasing concentrations of MT.

$$\Delta G_{\text{solvation}} = G_{\text{polar}} + G_{\text{nonploar}} \quad (7)$$

$$\Delta G_{\text{nonploar}} = \gamma \Delta \text{SASA} + \beta \quad (8)$$

The $T\Delta S$ represents the change in entropy following ligand binding, which was previously overlooked due to the noncritical nature of the entropic effect in calculating ligand binding affinities (eq 4). The gas phase energy (ΔE_{gas}) comprises the sum of internal (ΔE_{int}), van der Waals (ΔE_{vdW}), and electrostatic (ΔE_{elec}) energies (eq 5). Internal energy (ΔE_{int}) pertains to bond vibrations, bond angles, and rotation of single bond torsional angles (eq 6). Solvation-free energy ($\Delta G_{\text{solvation}}$) encompasses polar ($\Delta G_{\text{polar}}$) and nonpolar ($\Delta G_{\text{nonpolar}}$) energy contributions (eq 7). The polar solvation GGB contribution was evaluated using the generalized Born (GB) solvation module with a dielectric constant of 1 for solutes and 80.0 for solvents. Nonpolar free energy contributions were calculated using eq 8, where the surface tension proportionality constant γ and the free energy of nonpolar solvation of a point solute, β, were set to 0.00542 kcal/mol/Å^2 and 0.92 kcal/mol, respectively. SASA corresponds to the polarizable area of soluble agents.

Principal Component Analysis. The principal component analysis (PCA) is an important technique for minimizing data dimensionality while preserving as much disparity as possible. This basic method is widely used to find and recognize a protein structure's main positive and negative patterns. The implementation of the PCA to MD trajectories explained the atomic fluctuations of the Cα atoms in the protein. The principal components are eigenvectors of the covariance matrix. The PCA is built on the 3N-dimensional covariance matrix with elements C_{ij} for coordinates i and j. By the following equation, the matrix elements of the positional covariance matrix C were determined:

$$C_i = \langle (q_i - \langle q_i \rangle)(q_j - \langle q_j \rangle) \rangle \ (i, j = 1, 2, ..., 3N) \quad (9)$$

The average is computed following superimposition with a reference structure using a least-squares fitting procedure to eliminate translational and rotational motions. This helps isolate the significant motions from the MD trajectories. The Cartesian coordinates q_i and q_j represent the ith and jth C$^\alpha$ atom positions, respectively, with N denoting the total number of Cα atoms. Next, to obtain the eigenvalues and eigenvectors, the symmetric matrix C is converted into a diagonal matrix Λ of eigenvalues through an orthogonal coordinate transformation matrix T:

$$\Lambda = T^{\text{T}} C_{ij} T \quad (10)$$

The eigenvectors indicate the directions of motion relative to reference position q_i, with each eigenvector paired with an eigenvalue representing the overall mean-square fluctuation along that specific direction. The PCA was conducted using the CPPTRAJ module from the Amber 18 suite, and the protein's collective motions were visualized using a porcupine plot generated by NMWiz within VMD.[53]

RESULTS AND DISCUSSION

Dysregulation of signaling pathways, either directly or indirectly, is frequently linked to most human cancer initiation and progression.[54,55] Protein kinases are one of the essential components of these signaling cascades and, therefore, have drawn substantial interest from researchers as promising targets in cancer therapeutics.[56,57] Cancer cells exhibit a distinct metabolic characteristic, wherein aerobic glycolysis becomes the primary mode of energy production, diverging from oxidative phosphorylation. This metabolic adaptation serves as a vital survival mechanism for cancer cells, allowing them to flourish even in challenging conditions such as hypoxia. Playing a crucial role in modulating the metabolic shift during cancer onset and development, PDK3 is an important therapeutic target.[1,19] Several studies have documented the up-regulation of PDK3 in diverse cancer types, and a direct association has been noted between increased PDK3 expression and the advancement of cancer.[17,58−60]

Natural compounds are known to exhibit anticancer properties. The compounds extracted from the plants and phytochemicals are known to exhibit a wide range of biological activities.[61−64] In this study, we used a naturally occurring

https://doi.org/10.1021/acsomega.4c03001
ACS Omega 2024, 9, 29633−29643

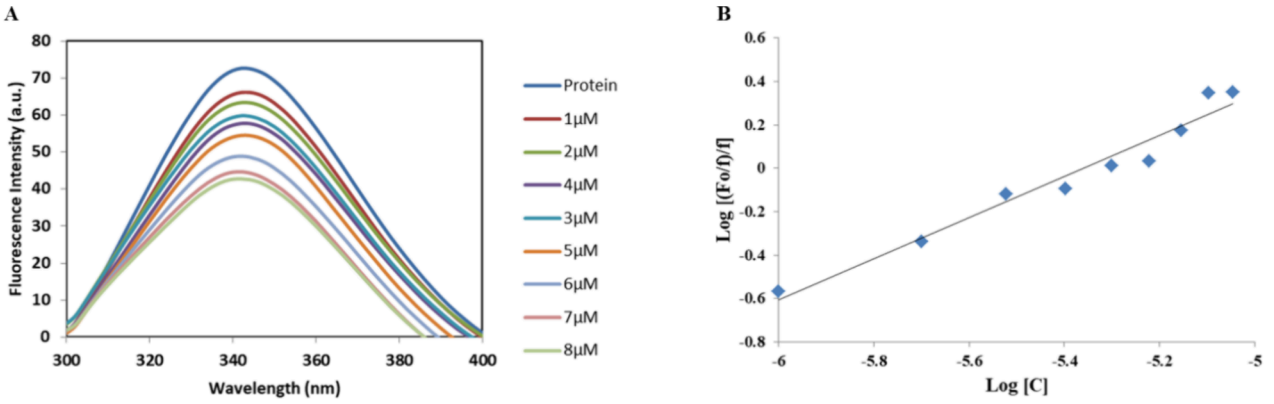

Figure 2. Fluorescence binding assay of MT binding to PDK3. (A) Fluorescence emission spectra of PDK3 with ascending concentration of MT (0 to 8 μM). (B) Modified Stern−Volmer (MSV) plot based on the fluorescence quenching of PDK3 as a function of increasing MT concentrations.

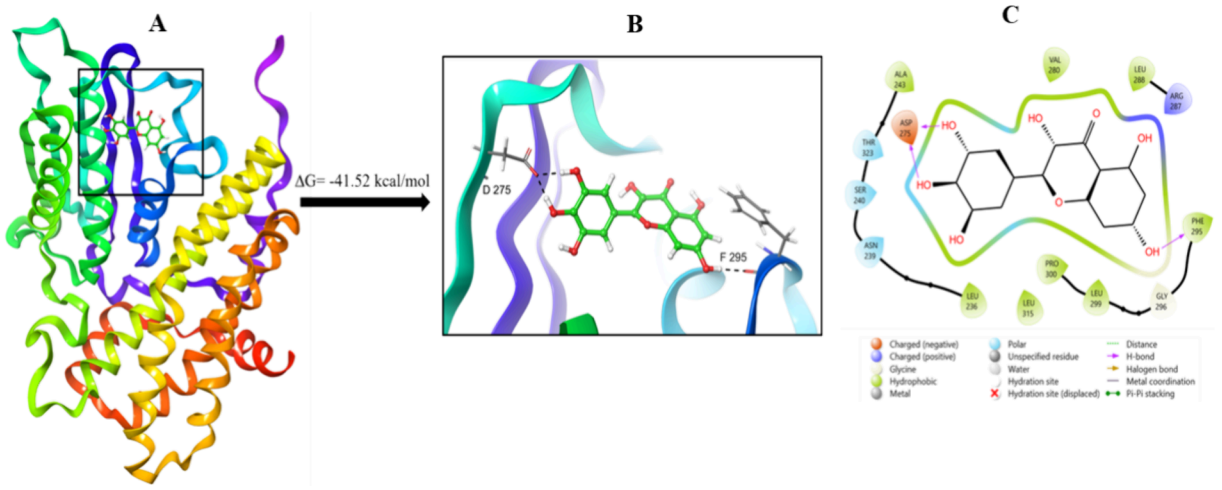

Figure 3. Structural representation of binding of PDK3 with MT. (A) Protein-MT complex. (B) A closer view of the binding site of PDK3 generating interactions with MT in 3-D orientation. (C) 2-D map of MT docked in complex with PDK3 protein showing hydrogen bonds and other associated interactions.

phytochemical MT and studied its effect on a protein kinase associated with cancer, PDK3. The ligand was studied for its binding potential, inhibitory potential, and binding affinity with PDK3. MT showed an effective binding with PDK3 in the active site pocket of the kinase domain. The ATPase assay depicted the kinase inhibitory potential of MT, and it was apparent that it showed a better IC_{50} value as compared to other phytochemicals that have been established as PDK3 inhibitors,[34,58] thereby implying MT is a more potent inhibitor. The binding of MT in the kinase domain was related to modulations in the structure and functional aspects of the protein. A detailed MD simulation was carried out for the apo-PDK3 and MT-PDK3 complexes, which showed the formation of a stable complex, predominated by a hydrogen bond. The MD simulation parameters showed the overall structural stability of the protein−ligand complex. The activity of the protein was decreased in the presence of the ligand in a concentration-dependent manner. The binding of MT with PDK3 showed an excellent binding affinity of the ligand toward the protein. The overall results depict that MT is an effective candidate in cancer therapeutics that inhibits the function of PDK3. Inhibition of overexpressed PDK3 may restore the dysregulated signaling cascade in cancer.

Enzyme Inhibition Assay. PDK3 exhibits ATPase activity, which can be utilized to evaluate the inhibitory capabilities of the ligands. The ATPase activity is the potential of the protein to hydrolyze ATP, and an experiment was carried out to estimate efficacy of MT in reducing the kinase activity of PDK3. We observed that MT exhibited a strong inhibitor of PDK3, has signficantly reduced its activity in a concentration-dependent manner, as depicted in Figure 1. The IC_{50} of MT against PDK3 was 3.3 μM.[65] The obtained IC_{50} value is much lower than that obtained for other phytochemicals that have been established as PDK3 inhibitors[29,58] in earlier published literature, thereby implying the significance of MT as a PDK3 inhibitor. Ligands can function as competitive inhibitors, binding to the active site of the kinase and impeding substrate binding. This competition for the active site disrupts the kinase's capability to phosphorylate its substrate, ultimately reducing its activity. Therefore, understanding these interactions is crucial for drug development and unraveling the intricate molecular mechanisms that underlie various biological processes.

Fluorescence Binding Studies. Fluorescence quenching is a phenomenon in which fluorophores emit emission spectra that decrease upon exposure to certain external factors or

https://doi.org/10.1021/acsomega.4c03001
ACS Omega 2024, 9, 29633−29643

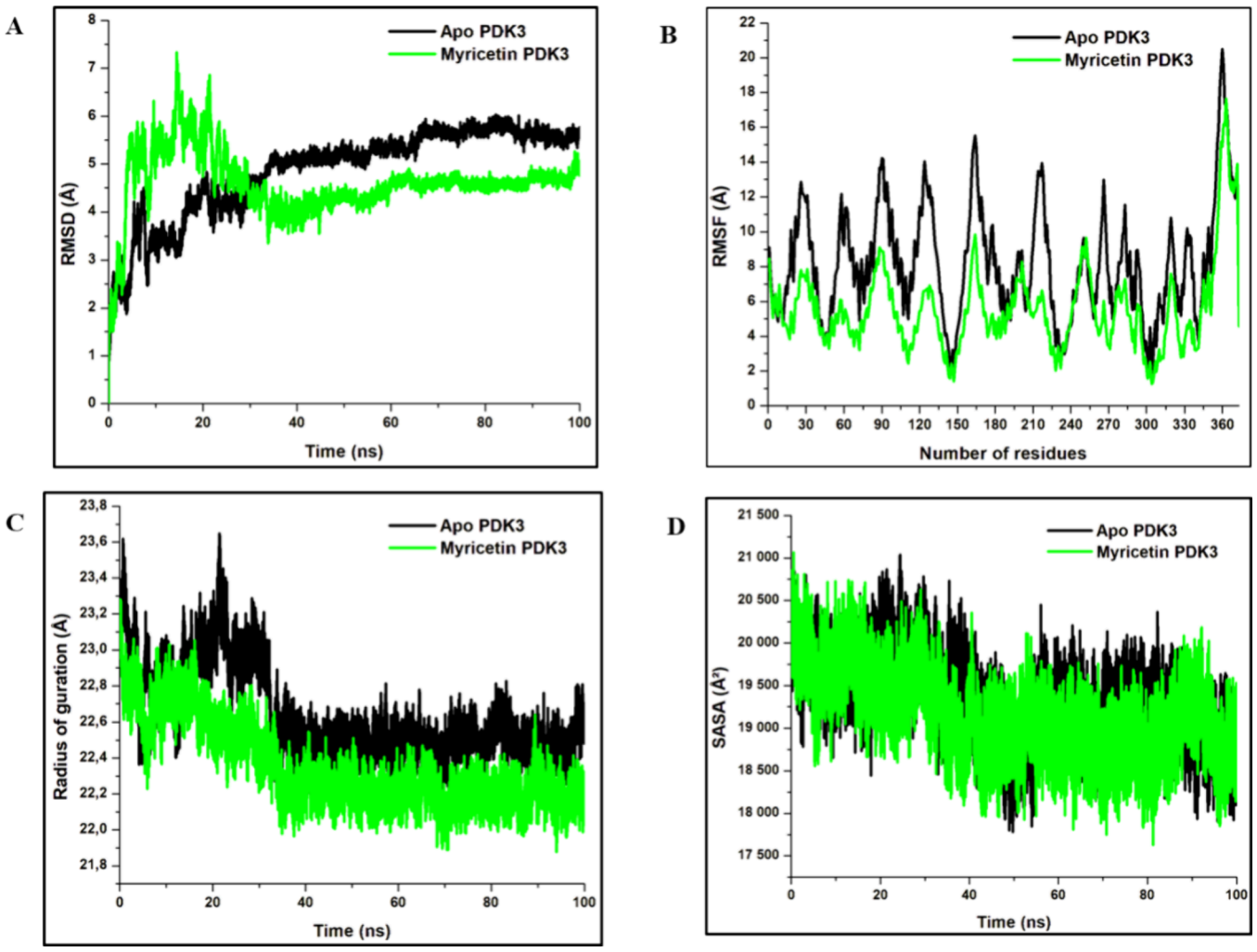

Figure 4. Structural dynamics of the PDK3 protein and in complex with MT. (A) RMSD in Å for C-backbone atoms of protein and protein−ligand complex; (B) RMSF values (Å) calculated for protein and protein−ligand complex; (C) R_g values (Å) after ligand binding and PDK3; (D) SASA values in Å^2 calculated for Apo-PDK3 and the MT-PDK3 complex after 100 ns of MD simulations.

interactions with other molecules. Fluorescence quenching can occur by three distinct mechanisms.[66,67]

An experiment on fluorescence quenching was performed featuring PDK3 as the fluorophore and MT as a quencher. The emission spectra indicated a decrease in fluorescence intensity upon addition of the ligand (ranging from 0 to 8 μM) to the protein. The change in fluorescence intensity was systematically investigated using the double log relation (modified Stern−Volmer equation) to assess the binding constant (K), as illustrated in Figure 2. The determined binding constant (K_a) for the MT-PDK3 complex was found to be 1.14×10^5 M^{-1}, which signifies a pronounced affinity between the protein and the ligand, highlighting the strength of their interaction.

Molecular Docking. In computer-aided drug development, molecular docking is a widely used to identify small molecules' preferred conformation or orientation in complexes with associated proteins. MT was docked at the active site of the PDK3 protein involving various binding forces. The outcome of docking is illustrated in Figures 3A and B. With a considerable docking score of −8.69 kcal/mol, the MT-PDK3 complex successfully showed positive orientations. MT engaged with the Asp275 residue of the PDK3 protein, forming a strong hydrogen bond contact via the benzene ring. The MT-PDK3 complex also engaged in an H-bond with Phe295. Additionally, MT was surrounded by several hydrophobic residues indicative of an accurate binding site. To support our theory, we carried out a thorough investigation of the MT-PDK3 complex.

Postdynamics Trajectory Analysis. We investigated structural parameters to evaluate the effect of MT binding to PDK3. The root-mean-square deviation (RMSD) was calculated to analyze the structural deviations and the modulation in dynamic behavior upon binding of the ligand to PDK3. A protein can exhibit various conformational alterations in its structure during the simulation. The changes majorly include reorganization of the side chains and a modified secondary structure that includes α-helices and β-sheets.[68] Apo-PDK3 protein and MT-PDK3 complex were shown to have average RMSDs of 4.89 and 4.29 Å, respectively. When compared with apo-PDK3, the MT-PDK3 complex showed a reduction in RMSD values. The RMSD of PDK3 shows the substantial stability of the MT-PDK3 complex, which is consistent with a noteworthy equilibration with no major changes after 30 ns of the MD simulation (Figure 4A).

Fluctuation of individual amino acid residues or groups of residues in a protein can be calculated in terms of root-mean-square fluctuation (RMSF). A variation of all of the residues

https://doi.org/10.1021/acsomega.4c03001
ACS Omega 2024, 9, 29633−29643

was calculated for both the MT-PDK3 complex and apo-PDK3, as shown in Figure 4B. The MT-PDK3 complex and apo-PDK3 were shown to have average RMSF values of 6.81 and 8.21 Å, respectively. An increased RMSF values without a ligand highlight notable structural variations during the simulation by indicating flexibility in specific regions. However, there was a minimal fluctuation in the protein residues were observed after MT binding. Numerous interactions, including hydrogen bonds and other noncovalent interactions were thought to contributed to the stability of this protein−ligand complex. Reduced protein fluctuation after MT binding indicates the strong stability of protein-ligand complex.

The radius of gyration (R_g) is used in analyzing the flexibility and compactness of a 3-D structure of a protein. The structural changes incurred upon ligand binding cause variations in the R_g values, which in turn cause protein folding or unfolding.[69] After estimating the R_g values, the digital values for the apo PDK3 and MT-PDK3 complex were calculated as 22.71 and 22.31 Å, respectively. Figure 4C illustrates the compactness in the MT-PDK3 complex. A compact and rounded system has a lower R_g value, which indicates packing closer to the center of mass and compactness of the atoms.

The surface area of a biomolecule accessible to solvent molecules is measured by the SASA estimate, which is essential for trajectory analysis generated by MD simulations. SASA is used to analyze how a molecule interacts with its surroundings and to explore biomolecules' dynamics, stability, and conformational changes.[70,71] The SASA value of the MT-PDK3 complex and apo-PDK3 protein was determined to have a better understanding of the conformational changes that occurred in the simulation. SASA values for PDK3 were determined to be 19,592 Å^2 overall; however, Figure 4D illustrates little variation following ligand interaction, with values of 19,253 Å^2. The ligand often occupies a specific binding pocket on the protein's surface during the ligand-binding process. The drop in SASA may be a sign of the successful occupancy of the binding pocket, reducing the amount of solvent to which this area is exposed. Based on comprehensive structural research, it can be inferred that the protein in its ligand-bound state is more stable and effective in blocking PDK3.

Hydrogen Bond Analysis. Hydrogen bonds encompass the electrostatic attraction between a hydrogen atom, bound to an electronegative atom, such as oxygen or nitrogen, and another electronegative atom. Within a protein−ligand complex, these bonds establish specific interactions between distinct amino acid residues in the protein and functional groups on the ligand. This specificity is crucial for ensuring the precise and accurate binding of the ligand to the protein. It is an essential technique to comprehend the structural stability of a protein to analyze the intramolecular hydrogen bonds formed when a ligand binds to it. The formation of hydrogen bonds between the protein and the ligand leads to a reduction in free energy, making the complex more stable.[34,72] The MT-PDK3 complex shows an increase in the number of hydrogen bonds. The MT-PDK3 complex shows increased hydrogen bonds, with a maximum of 140−215, whereas apo-PDK3 unbound to any ligand showed fewer H-bonds (145−204), as depicted in Figure 5. An increase in intramolecular H-bonds upon binding of MT to PDK3 can have significant implications for the structural stability of the complex.

Dynamical Cross-Correlation Matrix. Movements inside a protein occur throughout various periods from femtoseconds to seconds. The time scale used to compile the correlation data affects the dynamic cross-correlation matrix (DCCM) as well. The inter-residue DCCM analysis investigated the correlated and anticorrelated motions in the apo-PDK3 and MT-PDK3 complex. Figure 6 shows the DCCM plots created for the apo-PDK3 and MT-PDK3 complex.[73,74] Red and blue represent the positive and negative correlations among the residues. According to the maps, there were multiple positive correlations in the MT-PDK3 complex compared to apo-PDK3, which can be noted in Figures 6A and B. This indicates that the MT-PDK3 complex shows promising residual motions after compound binding. The patterns of correlations across all graphs are clearly distinguished, implying that the motions of both apo-PDK3 and its ligand-bound complex are stable.

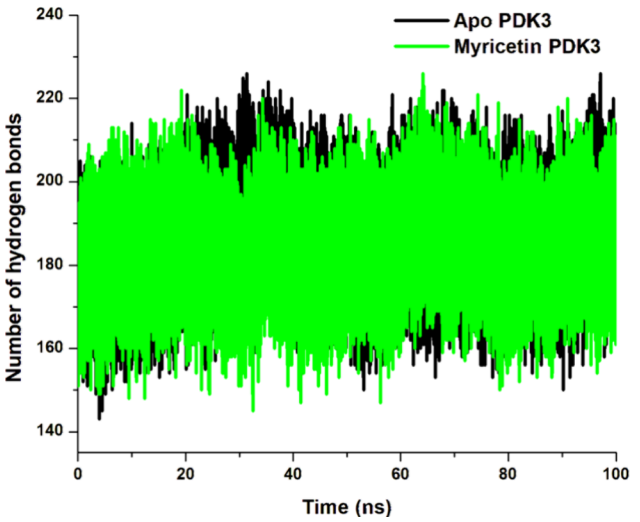

Figure 5. 2-D representation of intramolecular hydrogen bond formation for apo PDK3 and PDK3 in complex with MT over 100 ns of MD simulations.

MM/GBSA Free Binding Energy. To calculate the binding free energy of MT with the PDK3 protein, MM/GBSA was utilized. The results are displayed in Table 1. The MT-PDK3 complex's total binding free energy (ΔG_{bind}) was observed to have a digital value of −41.52 kcal/mol. A larger negative ΔG_{bind} shows a greater affinity for binding between the ligand and PDK3. The van der Waals energy shift upon protein−ligand binding is shown by the ΔE_{vdW} energy. With a binding score of −29.63 kcal/mol, the van der Waals energies in the MT-PDK3 complex contributed significantly. In addition to estimating overall binding free energy (ΔG_{bind}), the ΔE_{ele} gives information about the repulsive and attractive electrostatic interactions in ligand binding. MT-PDK3 complex stability was greatly aided by ΔE_{ele}, with a score of −72.39 kcal/mol. The ΔG_{gas} in the MT-PDK3 complex reflected a negative energy, with a score of −102.3 kcal/mol. The binding of MT with PDK3 was positively influenced by gas-phase interactions, as shown by the negative ΔG_{gas} values.

With a score of 60.51 kcal/mol, the MT-PDK3 complex showed positive scores of ΔG_{sol}. The result showed fewer contributions from solvation effects in the MT-PDK3 complex than the unbound solvation energy. With a 65.68 kcal/mol value, ΔG_{polar} showed a positive value for the protein−ligand complex, indicating less favorable contributions from the interactions. $\Delta G_{nonpolar}$ provides insight into the function of nonpolar solvation effects in ligand binding, such as van der Waals interactions and the hydrophobic effect. The value of

https://doi.org/10.1021/acsomega.4c03001
ACS Omega 2024, 9, 29633−29643

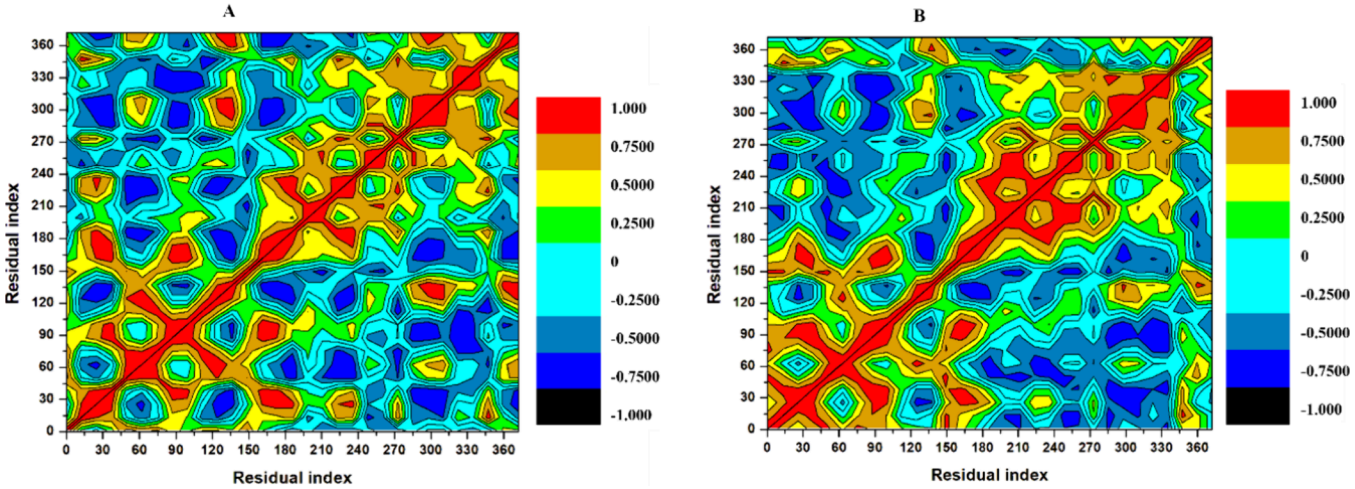

Figure 6. Two-dimensional distance correlation matrix for positive and negative correlation for (A) apo-PDK3 protein and (B) the protein in complex with MT after 100 ns of MD simulations.

Table 1. Binding free energy calculations of PDK3-MT complex using MM/GBSA approach.

Protein−ligand complex	ΔE_{vdW}	ΔE_{ele}	ΔG_{gas}	ΔG_{polar}	$\Delta G_{nonpolar}$	ΔG_{sol}	ΔG_{bind}
MT-PDK3	−29.63	−72.39	−102.03	65.68	−5.17	60.51	−41.52

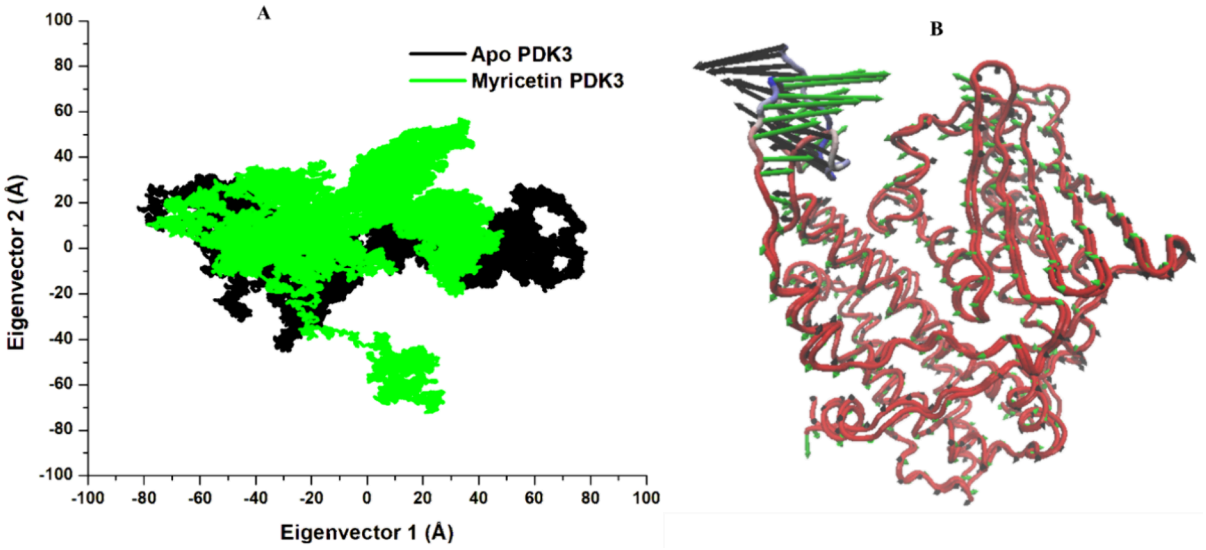

Figure 7. (A) PCA plot constructed by eigenvector 1 vs eigenvector 2 for apo-PDK3 and for PDK3-MT complex showing the positive and negative residual movements. (B) Relative projection of crystal structure with the initial coordinates of the simulations onto PC1−PC2 over 100 ns MD.

$\Delta G_{nonpolar}$, which is −5.17 kcal/mol, indicates that nonpolar solvation effects have contributed to favorable binding of MT to PDK3. This binding affinity data show that MT is a strong PDK3 inhibitor.

Principal Component Analysis. Based on eigenvectors on the X and Y axes, principal component analysis (PCA) was used to investigate the conformational changes in amino acids upon ligand interaction.[75] The 2-D Figure 7 illustrates the constant dispersion of MT in the PC1−PC2 locations. While MT was dispersed in positive locations on PC1−PC2 eigenvectors, apo-PDK3 was dispersed in negative locations on PC1. The proposed MT inhibitor demonstrated the most positive motions on both axes of eigenvector 2. Additionally, it showed a positive 20.21 Å trace covariance matrix with positive values on the *X*-axis. MT showed that upon binding to the PDK3 protein, there was a slight variation on eigenvectors 1 and 2, both of which had positive values. This investigation validates the residual fluctuations of the MT-PDK3 complex and apo-PDK3 that were previously indicated during the MD simulation.

CONCLUSIONS

This research emphasizes the vital role of protein kinases, with a particular focus on PDK3, in driving cancer progression by participating in metabolic modulations that enhance cancer survival. The direct correlation between overexpressed PDK3 and cancer indicates its role as potential drug target in cancer therapeutics. We investigated the inhibitory potential of MT against PDK3 using molecular docking, MD simulations, and activity assays and revealed a strong affinity of MT for PDK3.

https://doi.org/10.1021/acsomega.4c03001
ACS Omega 2024, 9, 29633−29643

MT significantly inhibited the enzymatic activity of PDK3 with an IC_{50} of 3.3 μM. A fluorescence binding assay also showed a high affinity of the MT towards PDK3. Further, MD simulation was carried out to understand the interactions of ligand molecule with PDK3. The MD simulation studies showed a stable MT-PDK3 complex formation. The complex was stabilized by van der Waals and electrostatic interactions; however, solvation energy did not contribute to the stability. Intramolecular hydrogen bonds contributed significantly to stabilizing the complex, with minimal conformational fluctuations throughout the simulation. Given the proven effectiveness of MT in inhibiting PDK3, it holds promise as a potential drug candidate for diseases linked to PDK3 dysregulation, after essential validations in clinical settings.

■ ASSOCIATED CONTENT

Data Availability Statement

All data generated or analyzed during this study are included in this article.

■ AUTHOR INFORMATION

Corresponding Authors

Md. Imtaiyaz Hassan − *Centre for Interdisciplinary Research in Basic Sciences, Jamia Millia Islamia, New Delhi 110025, India;* orcid.org/0000-0002-3663-4940; Email: mihassan@jmi.ac.in

Anas Shamsi − *Centre of Medical and Bio-Allied Health Sciences Research, Ajman University, Ajman 364, United Arab Emirates;* orcid.org/0000-0001-7055-7056; Email: anas.shamsi18@gmail.com

Authors

Saleha Anwar − *Centre for Interdisciplinary Research in Basic Sciences, Jamia Millia Islamia, New Delhi 110025, India*

Shama Khan − *South African Medical Research Council, Vaccines and Infectious Diseases Analytics Research Unit, Faculty of Health Science, School of Pathology, University of the Witwatersrand, Johannesburg 2193, South Africa*

Afzal Hussain − *Department of Pharmacognosy, College of Pharmacy, King Saud University, Riyadh 4545, Saudi Arabia*

Mohamed F. Alajmi − *Department of Pharmacognosy, College of Pharmacy, King Saud University, Riyadh 4545, Saudi Arabia*

Complete contact information is available at: https://pubs.acs.org/10.1021/acsomega.4c03001

Author Contributions

All authors have read and agreed to publish the current version of the manuscript. Saleha Anwar: Investigation, Data curation, Validation, Writing−original draft, Shama Khan: Data curation, Writing−review and editing. Afzal Hussain: Validation, Formal analysis, Mohamed F. Alajmi: Writing−review and editing, Anas Shamsi: Data curation, Validation, Formal analysis, Writing−review and editing, Md. Imtaiyaz Hassan: Funding acquisition, Conceptualization, Supervision, Project administration, Writing−review and editing.

Notes

The authors declare no competing financial interest.

■ ACKNOWLEDGMENTS

This work is supported by Central Council for Research in Unani Medicine (CCRUM), Ministry of AYUSH, Government of India (Grant No. 3-69/2020- CCRUM/Tech). MIH acknowledges the Council of Scientific and Industrial Research for financial support [Project No. 27(0368)/20/EMR-II]. AH acknowledges the generous support from the Researchers Supporting Project Number (RSPD2024 R980), King Saud University, Riyadh, Saudi Arabia. A.S. acknowledges Ajman University for supporting this publication.

■ LIST OF ABBREVIATIONS

PDK3,Pyruvate dehydrogenase kinase 3; ROS,Reactive oxygen species; FEL,Free energy landscape; MD,Molecular dynamics; PCA,Principal component analysis; R_g,Radius of gyration; RMSD,Root-mean-square deviation; RMSF,Root-mean-square fluctuation; SASA,Solvent accessible surface area; OXPHOS,Oxidative phosphorylation; ATP,Adenosine triphosphate; PDHC,Pyruvate dehydrogenase complex; HIF,1α-Hypoxia-inducible factor-1α

■ REFERENCES

(1) Anwar, S.; Shamsi, A.; Mohammad, T.; Islam, A.; Hassan, M. I. Targeting pyruvate dehydrogenase kinase signaling in the development of effective cancer therapy. *Biochimica et Biophysica Acta (BBA)-Reviews on Cancer* **2021**, *1876* (1), No. 188568.

(2) Koppenol, W. H.; Bounds, P. L.; Dang, C. V. Otto Warburg's contributions to current concepts of cancer metabolism. *Nature reviews cancer* **2011**, *11* (5), 325−337.

(3) Ji, K.; Mayernik, L.; Moin, K.; Sloane, B. F. Acidosis and proteolysis in the tumor microenvironment. *Cancer and Metastasis Reviews* **2019**, *38*, 103−112.

(4) Schwartz, L.; Supuran, C.; Alfarouk, K. The Warburg effect and the hallmarks of cancer. *Anti-Cancer Agents in Medicinal Chemistry* **2017**, *17* (2), 164−170.

(5) Alfarouk, K. O.; Stock, C.-M.; Taylor, S.; et al. Resistance to cancer chemotherapy: failure in drug response from ADME to P-gp. *Cancer cell international* **2015**, *15* (1), 1−13.

(6) Taylor, S. S.; Kornev, A. P. Protein kinases: evolution of dynamic regulatory proteins. *Trends in biochemical sciences* **2011**, *36* (2), 65−77.

(7) Hunter, T.; Cooper, J. A. Protein-tyrosine kinases. *Annual review of biochemistry* **1985**, *54* (1), 897−930.

(8) Ambinder, R. F. A viral protein kinase drug target for tumors? *J. Clin. Invest.* **2018**, *128* (6), 2197−2198.

(9) Ferguson, F. M.; Gray, N. S. Kinase inhibitors: the road ahead. *Nat. Rev. Drug Discovery* **2018**, *17* (5), 353−377.

(10) Wu, P.; Nielsen, T. E.; Clausen, M. H. Small-molecule kinase inhibitors: an analysis of FDA-approved drugs. *Drug Discovery Today* **2016**, *21* (1), 5−10.

(11) Qi, W.; Keenan, H. A.; Li, Q.; et al. Pyruvate kinase M2 activation may protect against the progression of diabetic glomerular pathology and mitochondrial dysfunction. *Nature medicine* **2017**, *23* (6), 753−762.

(12) Gao, Y.-L., Wang, N., Sun, F.-R., Cao, X.-P., Zhang, W., Yu, J.-T. Tau in neurodegenerative disease. *Annals of translational medicine* **2018**, *6* (10), 175.

(13) Roskoski, R., Jr. Properties of FDA-approved small molecule protein kinase inhibitors. *Pharmacological research* **2019**, *144*, 19−50.

(14) Steussy, C. N.; Popov, K. M.; Bowker-Kinley, M. M.; Sloan, R. B.; Harris, R. A.; Hamilton, J. A. Structure of pyruvate dehydrogenase kinase: novel folding pattern for a serine protein kinase. *J. Biol. Chem.* **2001**, *276* (40), 37443−37450.

(15) Harris, R. A.; Huang, B.; Wu, P. Control of pyruvate dehydrogenase kinase gene expression. *Advances in enzyme regulation* **2001**, *41* (1), 269−288.

(16) Baker, J. C.; Yan, X.; Peng, T.; Kasten, S.; Roche, T. E. Marked differences between two isoforms of human pyruvate dehydrogenase kinase. *J. Biol. Chem.* **2000**, *275* (21), 15773−15781.

(17) Lu, C.-W.; Lin, S.-C.; Chien, C.-W.; et al. Overexpression of pyruvate dehydrogenase kinase 3 increases drug resistance and early recurrence in colon cancer. *American journal of pathology* **2011**, *179* (3), 1405−1414.
(18) Lu, C.-W.; Lin, S.-C.; Chen, K.-F.; Lai, Y.-Y.; Tsai, S.-J. Induction of pyruvate dehydrogenase kinase-3 by hypoxia-inducible factor-1 promotes metabolic switch and drug resistance. *J. Biol. Chem.* **2008**, *283* (42), 28106−28114.
(19) Stacpoole, P. W. Therapeutic targeting of the pyruvate dehydrogenase complex/pyruvate dehydrogenase kinase (PDC/PDK) axis in cancer. *JNCI: Journal of the National Cancer Institute* **2017**, *109* (11), No. djx071.
(20) Woolbright, B. L.; Rajendran, G.; Harris, R. A.; Taylor, J. A., III Metabolic flexibility in cancer: targeting the pyruvate dehydrogenase kinase: pyruvate dehydrogenase axis. *Molecular cancer therapeutics* **2019**, *18* (10), 1673−1681.
(21) Mohammad, T.; Arif, K.; Alajmi, M. F.; et al. Identification of high-affinity inhibitors of pyruvate dehydrogenase kinase-3: towards therapeutic management of cancer. *J. Biomol. Struct. Dyn.* **2021**, *39* (2), 586−594.
(22) Naz, F.; Khan, F. I.; Mohammad, T.; et al. Investigation of molecular mechanism of recognition between citral and MARK4: A newer therapeutic approach to attenuate cancer cell progression. *Int. J. Biol. Macromol.* **2018**, *107*, 2580−2589.
(23) Anwar, S.; Kar, R. K.; Haque, M. A.; et al. Effect of pH on the structure and function of pyruvate dehydrogenase kinase 3: Combined spectroscopic and MD simulation studies. *Int. J. Biol. Macromol.* **2020**, *147*, 768−777.
(24) Naz, H.; Khan, P.; Tarique, M.; et al. Binding studies and biological evaluation of β-carotene as a potential inhibitor of human calcium/calmodulin-dependent protein kinase IV. *Int. J. Biol. Macromol.* **2017**, *96*, 161−170.
(25) Adnan, M.; Anwar, S.; DasGupta, D.; et al. Targeting inhibition of microtubule affinity regulating kinase 4 by Harmaline: Strategy to combat Alzheimer's disease. *Int. J. Biol. Macromol.* **2023**, *224*, 188−195.
(26) Adnan, M.; DasGupta, D.; Anwar, S.; et al. Investigating role of plumbagin in preventing neurodegenerative diseases via inhibiting microtubule affinity regulating kinase 4. *J. Mol. Liq.* **2023**, *384*, No. 122267.
(27) Brami, C.; Bao, T.; Deng, G. Natural products and complementary therapies for chemotherapy-induced peripheral neuropathy: a systematic review. *Critical reviews in oncology/hematology* **2016**, *98*, 325−334.
(28) Anwar, S.; Mohammad, T.; Azhar, M. K.; et al. Investigating MARK4 inhibitory potential of Bacopaside II: Targeting Alzheimer's disease. *Int. J. Biol. Macromol.* **2023**, *245*, No. 125364.
(29) Anwar, S.; DasGupta, D.; Shafie, A.; et al. Implications of tempol in pyruvate dehydrogenase kinase 3 targeted anticancer therapeutics: Computational, spectroscopic, and calorimetric studies. *J. Mol. Liq.* **2022**, *350*, No. 118581.
(30) Rahmani, A. H.; Almatroudi, A.; Allemailem, K. S.; et al. Myricetin: A significant emphasis on its anticancer potential via the modulation of inflammation and signal transduction pathways. *International Journal of Molecular Sciences* **2023**, *24* (11), 9665.
(31) Imran, M.; Saeed, F.; Hussain, G.; et al. Myricetin: A comprehensive review on its biological potentials. *Food Science & Nutrition* **2021**, *9* (10), 5854−5868.
(32) Afroze, N.; Pramodh, S.; Hussain, A.; Waleed, M.; Vakharia, K. A review on myricetin as a potential therapeutic candidate for cancer prevention. *3 Biotech* **2020**, *10* (5), 211.
(33) Felice, M. R.; Maugeri, A.; De Sarro, G.; Navarra, M.; Barreca, D. Molecular pathways involved in the anti-cancer activity of flavonols: a focus on myricetin and kaempferol. *International Journal of Molecular Sciences* **2022**, *23* (8), 4411.
(34) Anwar, S.; Mohammad, T.; Shamsi, A.; et al. Discovery of Hordenine as a potential inhibitor of pyruvate dehydrogenase kinase 3: implication in lung Cancer therapy. *Biomedicines* **2020**, *8* (5), 119.
(35) Anwar, S.; DasGupta, D.; Azum, N.; et al. Inhibition of PDK3 by artemisinin, a repurposed antimalarial drug in cancer therapy. *J. Mol. Liq.* **2022**, *355*, No. 118928.
(36) Chi, Z.; Liu, R. Phenotypic characterization of the binding of tetracycline to human serum albumin. *Biomacromolecules* **2011**, *12* (1), 203−209.
(37) Shamsi, A.; Anwar, S.; Mohammad, T.; et al. MARK4 inhibited by AChE inhibitors, donepezil and Rivastigmine tartrate: insights into Alzheimer's disease therapy. *Biomolecules* **2020**, *10* (5), 789.
(38) Kato, M.; Chuang, J. L.; Tso, S. C.; Wynn, R. M.; Chuang, D. T. Crystal structure of pyruvate dehydrogenase kinase 3 bound to lipoyl domain 2 of human pyruvate dehydrogenase complex. *EMBO journal* **2005**, *24* (10), 1763−1774.
(39) Harder, E.; Damm, W.; Maple, J.; et al. OPLS3: a force field providing broad coverage of drug-like small molecules and proteins. *J. Chem. Theory Comput.* **2016**, *12* (1), 281−296.
(40) Madhavi Sastry, G.; Adzhigirey, M.; Day, T.; Annabhimoju, R.; Sherman, W. Protein and ligand preparation: parameters, protocols, and influence on virtual screening enrichments. *Journal of computer-aided molecular design* **2013**, *27*, 221−234.
(41) Friesner, R. A.; Banks, J. L.; Murphy, R. B.; et al. Glide: a new approach for rapid, accurate docking and scoring. 1. Method and assessment of docking accuracy. *Journal of medicinal chemistry* **2004**, *47* (7), 1739−1749.
(42) Maier, J. A.; Martinez, C.; Kasavajhala, K.; Wickstrom, L.; Hauser, K. E.; Simmerling, C. ff14SB: improving the accuracy of protein side chain and backbone parameters from ff99SB. *J. Chem. Theory Comput.* **2015**, *11* (8), 3696−3713.
(43) Khan, S.; Alhumaydhi, F. A.; Khan, M. S.; et al. Exploring binding mechanism of naringenin to human transferrin using combined spectroscopic and computational methods: Towards therapeutic targeting of neurodegenerative diseases. *J. Mol. Liq.* **2022**, *356*, No. 119001.
(44) Lee, T.-S.; Cerutti, D. S.; Mermelstein, D.; et al. GPU-accelerated molecular dynamics and free energy methods in Amber18: performance enhancements and new features. *J. Chem. Inf. Model.* **2018**, *58* (10), 2043−2050.
(45) Perez, A.; MacCallum, J. L.; Brini, E.; Simmerling, C.; Dill, K. A. Grid-based backbone correction to the ff12SB protein force field for implicit-solvent simulations. *J. Chem. Theory Comput.* **2015**, *11* (10), 4770−4779.
(46) Khan, S.; Madhi, S. A.; Olwagen, C. Structure-based identification of novel inhibitors targeting the enoyl-ACP reductase enzyme of Acinetobacter baumannii. *Sci. Rep.* **2023**, *13* (1), No. 21331.
(47) Roe, D. R.; Cheatham, T. E., III PTRAJ and CPPTRAJ: software for processing and analysis of molecular dynamics trajectory data. *J. Chem. Theory Comput.* **2013**, *9* (7), 3084−3095.
(48) Seifert, E. OriginPro 9.1: scientific data analysis and graphing software-software review. *J. Chem. Inf. Model.* **2014**, *54* (5), 1552.
(49) Fataftah, H.; Karain, W. Detecting protein atom correlations using correlation of probability of recurrence. *Proteins: Struct., Funct., Bioinf.* **2014**, *82* (9), 2180−2189.
(50) Shafie, A.; Khan, S.; Zehra.; et al. Identification of phytoconstituents as potent inhibitors of casein kinase-1 alpha using virtual screening and molecular dynamics simulations. *Pharmaceutics* **2021**, *13* (12), 2157.
(51) Wang, E.; Sun, H.; Wang, J.; et al. End-point binding free energy calculation with MM/PBSA and MM/GBSA: strategies and applications in drug design. *Chem. Rev.* **2019**, *119* (16), 9478−9508.
(52) Anwar, S.; Khan, S.; Anjum, F.; et al. Myricetin inhibits breast and lung cancer cells proliferation via inhibiting MARK4. *Journal of Cellular Biochemistry* **2022**, *123* (2), 359−374.
(53) Humphrey, W.; Dalke, A.; Schulten, K. VMD: visual molecular dynamics. *J. Mol. Graphics* **1996**, *14* (1), 33−38.
(54) Kumari, M.; Chhikara, B. S.; Singh, P.; Rathi, B.; Singh, G. Signaling and molecular pathways implicated in oral cancer: A concise review. *Chemical Biology Letters* **2024**, *11* (1), 652−652.

https://doi.org/10.1021/acsomega.4c03001
ACS Omega 2024, 9, 29633−29643

(55) Panwar, V.; Singh, A.; Bhatt, M.; et al. Multifaceted role of mTOR (mammalian target of rapamycin) signaling pathway in human health and disease. *Signal transduction and targeted therapy* **2023**, *8* (1), 375.
(56) Brognard, J.; Hunter, T. Protein kinase signaling networks in cancer. *Current opinion in genetics & development* **2011**, *21* (1), 4−11.
(57) Dhillon, A. S.; Hagan, S.; Rath, O.; Kolch, W. MAP kinase signalling pathways in cancer. *Oncogene* **2007**, *26* (22), 3279−3290.
(58) Dahiya, R.; Mohammad, T.; Roy, S.; et al. Investigation of inhibitory potential of quercetin to the pyruvate dehydrogenase kinase 3: Towards implications in anticancer therapy. *Int. J. Biol. Macromol.* **2019**, *136*, 1076−1085.
(59) Criollo-Mendoza, M. S.; Contreras-Angulo, L. A.; Leyva-López, N.; Gutiérrez-Grijalva, E. P.; Jiménez-Ortega, L. A.; Heredia, J. B. Wound healing properties of natural products: Mechanisms of action. *Molecules* **2023**, *28* (2), 598.
(60) Rahaman, M. M.; Hossain, R.; Herrera-Bravo, J.; et al. Natural antioxidants from some fruits, seeds, foods, natural products, and associated health benefits: An update. *Food Science & Nutrition* **2023**, *11* (4), 1657−1670.
(61) Gupta, M.; Mishra, V.; Gulati, M.; et al. Natural compounds as safe therapeutic options for ulcerative colitis. *Inflammopharmacology* **2022**, *30* (2), 397−434.
(62) Diniz do Nascimento, L.; Barbosa de Moraes, A. A.; Santana da Costa, K.; et al. Bioactive natural compounds and antioxidant activity of essential oils from spice plants: New findings and potential applications. *Biomolecules* **2020**, *10* (7), 988.
(63) Wigner, P.; Bijak, M.; Saluk-Bijak, J. The green anti-cancer weapon. The role of natural compounds in bladder cancer treatment. *International Journal of Molecular Sciences* **2021**, *22* (15), 7787.
(64) Das, P. K.; Zahan, T.; Rakib, A.; Khanam, J. A.; Pillai, S.; Islam, F. Natural compounds targeting cancer stem cells: a promising resource for chemotherapy. *Anti-Cancer Agents in Medicinal Chemistry (Formerly Current Medicinal Chemistry-Anti-Cancer Agents)* **2019**, *19* (15), 1796−1808.
(65) Inc. AB. IC50 Calculator. 2024; https://www.aatbio.com/tools/ic50-calculator.
(66) Wang, Q.; Huang, C-r; Jiang, M.; et al. Binding interaction of atorvastatin with bovine serum albumin: Spectroscopic methods and molecular docking. *Spectrochimica Acta Part A: Molecular and Biomolecular Spectroscopy* **2016**, *156*, 155−163.
(67) Zhang, Y.-F.; Zhou, K.-L.; Lou, Y.-Y.; Pan, D-q; Shi, J.-H. Investigation of the binding interaction between estazolam and bovine serum albumin: multi-spectroscopic methods and molecular docking technique. *J. Biomol. Struct. Dyn.* **2017**, *35* (16), 3605−3614.
(68) Kuzmanic, A.; Zagrovic, B. Determination of ensemble-average pairwise root mean-square deviation from experimental B-factors. *Biophysical journal* **2010**, *98* (5), 861−871.
(69) Beg, A.; Khan, F. I.; Lobb, K. A.; Islam, A.; Ahmad, F.; Hassan, M. I. High throughput screening, docking, and molecular dynamics studies to identify potential inhibitors of human calcium/calmodulin-dependent protein kinase IV. *J. Biomol. Struct. Dyn.* **2019**, *37* (8), 2179−2192.
(70) Rodier, F.; Bahadur, R. P.; Chakrabarti, P.; Janin, J. Hydration of protein−protein interfaces. *Proteins: Struct., Funct., Bioinf.* **2005**, *60* (1), 36−45.
(71) Ausaf Ali, S.; Hassan, I.; Islam, A.; Ahmad, F. A review of methods available to estimate solvent-accessible surface areas of soluble proteins in the folded and unfolded states. *Current Protein and Peptide Science* **2014**, *15* (5), 456−476.
(72) Kuhn, B.; Mohr, P.; Stahl, M. Intramolecular hydrogen bonding in medicinal chemistry. *Journal of medicinal chemistry* **2010**, *53* (6), 2601−2611.
(73) Grimaldo, M.; Roosen-Runge, F.; Zhang, F.; Schreiber, F.; Seydel, T. Dynamics of proteins in solution. *Q. Rev. Biophys.* **2019**, *52*, No. e7.
(74) Mishra, S. K.; Jernigan, R. L. Protein dynamic communities from elastic network models align closely to the communities defined by molecular dynamics. *PloS one* **2018**, *13* (6), No. e0199225.
(75) Khan, S.; Madhi, S. A.; Olwagen, C. In-silico identification of potential inhibitors against FabI protein in Klebsiella pneumoniae. *J. Biomol. Struct. Dyn.* **2024**, *42*, 1−12.

https://doi.org/10.1021/acsomega.4c03001
ACS Omega 2024, 9, 29633−29643